Available online at www.sciencedirect.com

ScienceDirect

Procedia Computer Science 196 (2022) 151–158

Procedia Computer Science

www.elsevier.com/locate/procedia

CENTERIS - International Conference on ENTERprise Information Systems / ProjMAN - International Conference on Project MANagement / HCist - International Conference on Health and Social Care Information Systems and Technologies 2021

Deformation Fringes Detection in SAR interferograms Using Deep Learning

Bruno Silva[a], Joaquim J. Sousa[b,c,*], Milan Lazecky[d], António Cunha[b,c]

[a]*Faculdade de Ciências da Universidade do Porto,Porto 4169-007, Portugal*
[b]*Universidade de Trás-os-Montes e Alto Douro, Quinta de Prado, 5000-811 Vila Real, Portugal*
[c]*Instituto de Engenharia de Sistemas e Computadores, Tecnologia e Ciência, Porto 4200-465, Portugal*
[d]*COMET, School of Earth and Environment, University of Leeds*

Abstract

The success achieved by using SAR data in the study of the Earth led to a firm commitment from space agencies to develop more and better space-borne SAR sensors. This involvement of the space agencies makes us believe that it is possible to increase the potential of SAR interferometry (InSAR) to near real-time monitoring. Among this ever-increasing number of sensors, the ESA's Sentinel-1 (C-band) mission stands out and appears to be disruptive. This mission is acquiring vast volumes of data making current analyzing approaches inviable. This amount of data can no longer be analyzed and studied using classic methods raising the need to use and create new techniques. We believe that Machine Learning techniques can be the solution to overcome this issue since they allow to train Deep Learning models to automate human processes for a vast volume of data. In this paper, we use deep learning models to automatically find and locate deformation areas in InSAR interferograms without atmospheric correction. We train three state-of-the-art classification models for detection deformation areas, achieving an AUC of 0.864 for the best model (VGG19 for wrapped interferograms). Additionally, we use the same models as encoders to train U-net models, achieving a Dice score of 0.54 for InceptionV3. It is necessary more data to achieve better results in segmentation.

Keywords: Deep learning; Deformation Fringes; InSAR.

* Corresponding author.
E-mail address: jjsousa@utad.pt.

10.1016/j.procs.2021.11.084

1. Introduction

A synthetic aperture radar (SAR) sensor transmits electromagnetic waves at a wavelength ranging from a few millimeters to tens of centimeters. It can operate day and night under all weather conditions. SAR interferometry (InSAR) uses the phase of the signal from two or more SAR images covering the same area to extract landscape topography and its deformation patterns[1], [2]. Time-series InSAR data allow us to study the Earth's surface displacement in the long term. Changes in the Earth's surface can result from a wide range of phenomena such as earthquakes, volcanoes, landslides, variations in groundwater levels, and changes in wetland water levels [3]. With the evolution of technology and the success of InSAR, more SAR missions have been developed, which culminated in large amounts of data that can no longer be analyzed using manual-based methods. For example, the ESA's Sentinel-1 mission, the source from which the data in this work came, acquires more than 10Tb of data per day.

One way to effectively overcome this problem is to use deep learning algorithms to automatically detect deformation patterns in SAR interferograms. The "deep" in deep learning stands for the idea of successive layers of representations, and the depth of the model represents the number of layers contributing to a model [4]. The implementation of layers is usually obtained through a convolution neural network (CNN) that is placed sequentially. To start, it is needed to prepare the data that will be the input. Next, the data will pass for the layers, providing a response - at the first instance, it will be a random one -, then a comparison between the response given for the algorithm and the real response given by the input data is carried out, and its difference represents the loss score. In the end, this score will be used as a feedback signal to adjust the value of the layers' weights in a direction that will lower the loss score for the current example. This adjustment is the job of an optimizer. This process is recursively applied until the best possible answer is obtained [5].

Convolutional Neural Network is a class of artificial neural network (ANN) that has been used successfully in the processing and analysis of digital images. Like other Neural Networks, CNNs have an input, an output, and hidden layers, the difference is that the hidden layers are essential 2D Convolutional layers (Conv2D), which are 2D tensors [4]. CNNs are capable of finding patterns in images. These layers use filters in convolutional layers leading to a sharp increase in the amount of data processed in the network. In addition, the pooling layer of max-pooling in some considered neighborhoods is used to reduce them [6].

The application of deep learning in InSAR is recent, having found only two studies where machine learning was used to detect earthquake fringes [7]. However, there are some studies applied to detect deformation from others sources. These studies can be divided into two sub-themes, the use of machine learning to detect volcanic deformation [8]–[11] and the use of machine learning to detect slow ground deformation [12]–[16].

In this paper, two datasets (for wrapped and unwrapped interferograms) were created to automatically find deformation in both SAR wrapped and unwrapped interferograms without any type of atmospheric correction. For that, we test pre-trained CNNs for both types of interferograms. In the end, we use the same three models as an encoder to train a U-net model [17] for segmentation. In wrapped interferograms, deformations are characterized by fringes (Figure 1a), where each fringe corresponds to a deformation in the order of half of the signal's wavelength. These fringes can be more or less visible, depending on the scale of deformation, the difference in the dates of the two SAR images, or the amount of atmospheric noise. Unwrapped interferograms are usually associated with a color scale representing the displacement value (Figure 1b).

What makes earthquakes different from other types of deformation in interferograms is that in earthquakes, the fault that caused the earthquake is usually observed (Figure 1). However, this fault may not be visible when dealing with more minor deformations.

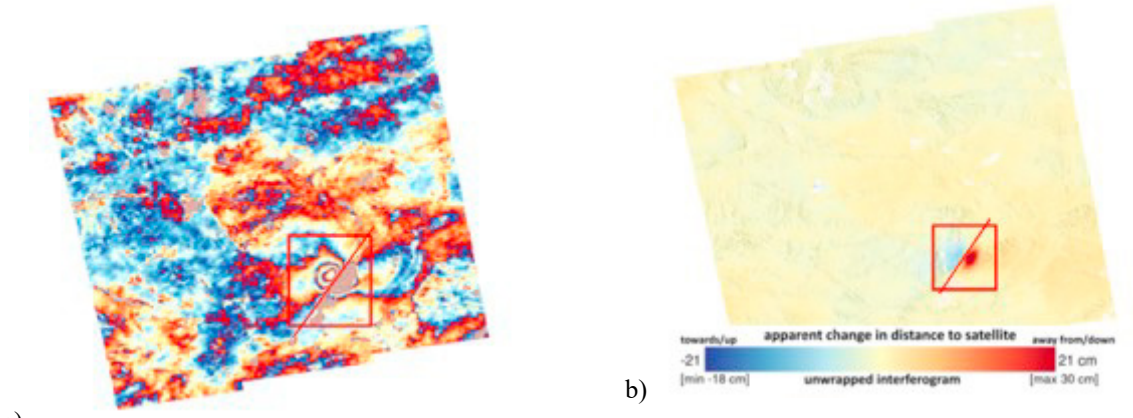

a) b)

Figure 1: Example of interferograms from the Xizang earthquake (2020): a) wrapped interferogram; b) unwrapped interferogram

2. Methods

The work presented in this paper is divided into three parts, as presented in Figure 2. First, we created the InSAR dataset and prepared the data to train the models. Then, we divided the data into three parts, originating three datasets: train, validation, and test sets. Next, we used the train and validation sets to train the classification and Segmentation models. Finally, we evaluated the models with the test set.

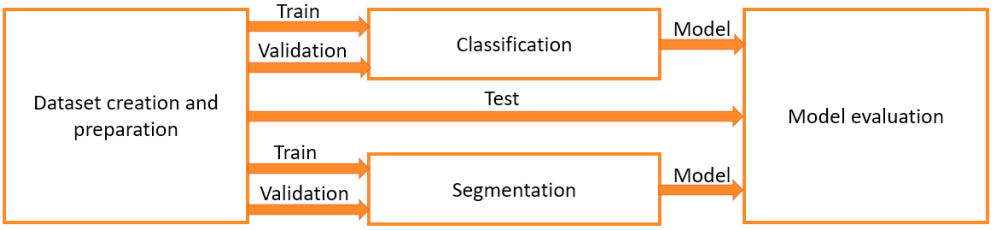

Figure 2:Description of the paper

InSAR dataset and data preparation

We used two datasets created by us for this work, one with wrapped interferograms and the other with unwrapped interferograms. All the data was obtained from the LiCS database from COMET (https://comet.nerc.ac.uk/comet-lics-portal/). We pick 29 zones where earthquakes occurred in the period span 2019-2021 and downloaded 3261 interferograms for each dataset. From these 3261, 469 represented positive cases, i.e. where deformation fringes are visible.

Initially, for each interferogram with deformation, we created a mask in Photoshop (a software from Adobe)[18] to use as input in the segmentation stage. From here, all the steps that we used to prepare the dataset were applied to masks, allowing each patch to have its corresponding mask. Then we divided the dataset into three parts: train set (~75% of the data), validation set (~15% of the data), and test set (~15% of the data).

The downloaded images did not all have the same dimension. Knowing that the area is the same for all interferograms, we decided to convert all the images to 1024×1024 pixels. These dimensions seemed to be the most suitable because these are intermediate values of what we obtain from the raw data and facilitates the creation of patches. With patches of 512x512 would have made it impossible to see small deformations in area, and 2048x2048 would have created a much more significant imbalance that would be a problem, in addition, could deform small images.

After this, we cut the images in patches of 256×256 pixels. For the cases without deformation fringes we cut into parallel patches (red ones in Figure 3). For the interferograms with deformation fringes we cut the patches into a stride of 128-pixel patches (Figure 3). Initially, we also tried parallel patches on images with deformation, but the poor results obtained due to patches with the fringes at the edges made us change the approach to guarantee the deformation in the patch center.

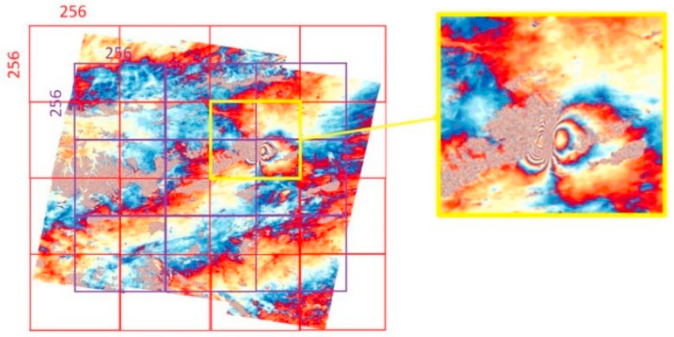

Figure 3: Interferogram divided into overlapped patches. Patches with more than 80% of the earthquake fringes were consider positive, those with 20% or less were discarded, and the remaining were consider negative (due to the number of negative cases, some of them were not used).

After the creation of patches, the dataset was unbalanced. The number of patches without deformation was considerably higher than the number of patches with deformation and to obtain the best results on deep learning models, data needs to be balanced. First, in the preliminary tests, we used Data Augmentation, creating synthetic data in patches with deformation fringes to balance the data, but when we increase the dataset downloading more real data, the imbalance started to get bigger, this technique started to perform worse. To overcome this problem, instead of Data Augmentation, we applied the focal loss [19] as the loss function. We end up with a balanced dataset, equally distributed for wrapped and unwrapped interferograms (Table 1).

Table 1: Final dataset used in the experiment.

	Train	Validation	Test*
Earthquake fringes (deformation)	499	380	252
No deformation	14979	4051	3826

Models Train

We used three pre-trained deep learning (InceptionV3[20], VGG19[21], and ResNet50V2[22]) models for both datasets for patches classification as earthquakes or not. For the input, we used the 256×256 pixels patches. For the output, it was used a sigmoid - the percentage of the patch containing deformation fringes. For the optimizer, we use Adam with a learning rate of 0.00001. We use 260 steps per epoch and 60 validation steps during 150 epochs. We use the callback "ModelCheckpoint" that only saves the best model according to the loss. We used the same models to train U-net models. Initially, in the encoder, we used the weights of the trained models in classification. Since the results were around 0, we decided to train the encoders again during the U-net model training.

3. Results

Four metrics were computed to evaluate the models for classification: ROC Curve [23], AUC, Accuracy (as 50% threshold), and F1 Score [24]. These metrics are summarized in Table 2 and Figure 4.

Table 2: Metrics for classification models

	Wrapped interferograms			Unwrapped interferograms		
Models	Accuracy	F1 Score	AUC	Accuracy	F1 Score	AUC
InceptionV3	0.95169	0.3706	0.768	0.938	0.1366	0.651
VGG19	0.9708	0.6909	0.864	0.9510	0.3299	0.7340
Resnet50V2	0. 96027	0.5263	0.752	0.9434	0.1596	0.669

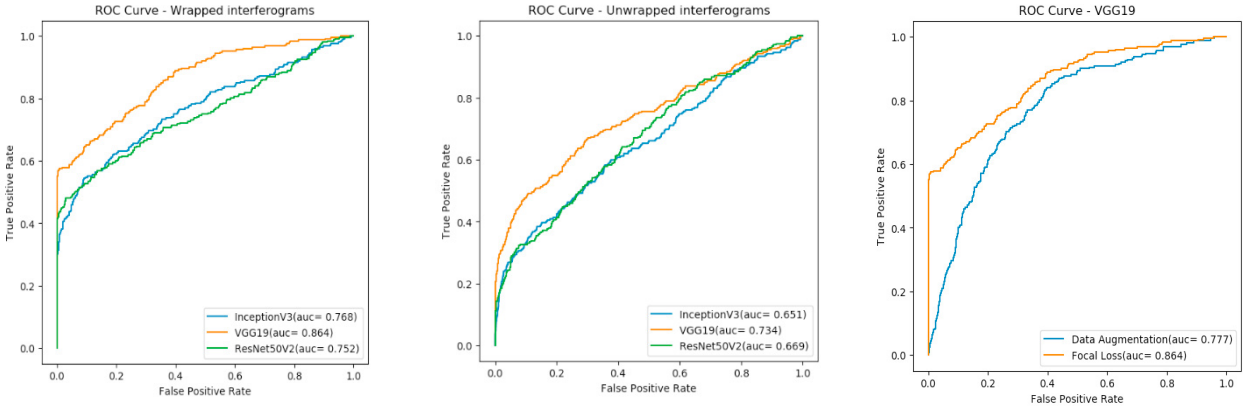

Figure 4: ROC Curves a) wrapped interferograms, b) unwrapped interferograms, c) comparison between Data Augmentation and Focal Loss for the best model (VGG19)

This dataset is very unbalanced. Though accuracy is very high compared with the other metrics in both models, that means that in this case, the accuracy is not a relevant metric. As expected, wrapped interferograms allowed better results compared to unwrapped interferograms. VGG19 became the best model for deformation detection in interferograms, as seen in ROC Curve (receiver operating characteristic curve) and AUC (Area Under the Curve).

Calculating the g-mean[25] for all thresholds in VGG19 for wrapped interferograms, we can see that the best threshold to find deformation fringes is 0.360 with a g-mean of 0.98 on the train set. On the other hand, the 0.5 threshold only has a g-mean of 0.92.

Focal loss performs better than data augmentation to deal with unbalanced data, as can be seen in Figure 4 c).

Overall, these results can be considered reasonable. However, in practice, the interferograms are cut into overlapped patches, and most of the time, the model did not detect the earthquake fringes in patches that changed in the overlapped patch. On the other side, each earthquake fringe is detected in several images/interferograms, ensuring that one patch is well detected in almost all cases, as shown in Figure 6.

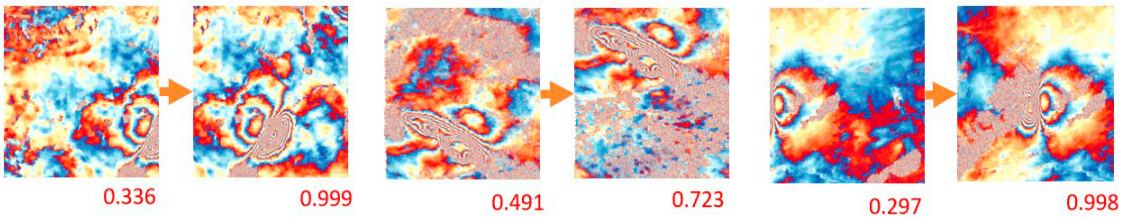

Figure 5: Overlapped earthquakes patches and its probability of having deformation earthquake according to the model

We used Intersection over Union Score [15], Dice Score[16], and Accuracy for the segmentation evaluation. The achieved results are presented in Table 3.

Table 3: Results for segmentation

Model	IoU Score	Dice Score	Accuracy
InceptionV3	0.4274	0.5896	0.8310
VGG19	0.3194	0.4746	0.8469
Resnet50	0.1268	0.2232	0.7968

The obtained results are poor. We tried several approaches, and we will need to gather more data to train the segment models properly. Some segmented images are presented in Figure 6.

The difficulty in detecting the edges between deformation/no deformation was revealed to be the main factor contributing to some errors in InceptionV3 segmentation. This effect can be seen in Figure 6 a, b. RegardingVGG19, the main constraint lies in the fact that VGG19 interprets the noise in images as deformation fringes (Figure 6 c, d).

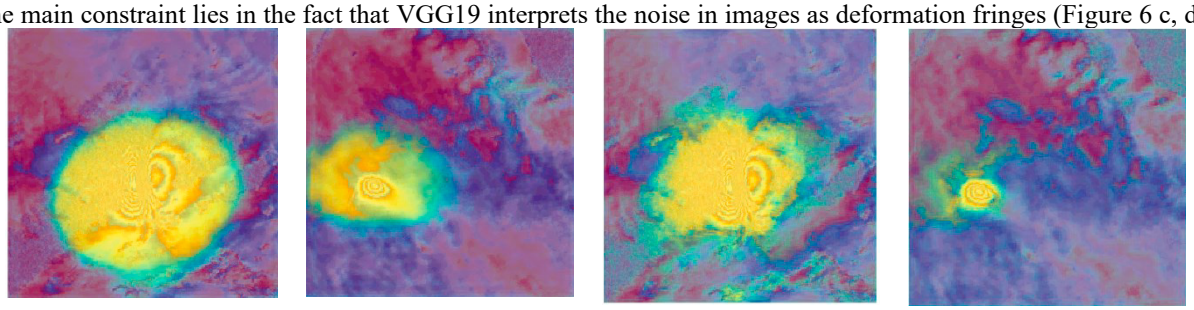

a) b) c) d)

Figure 6:Segmented area for two earthquakes using a,b) InceptionV3 c,d) VGG19

The results are very promising, but the dataset is too small and too unbalanced to allow better results. However, with a more extensive dataset and a deeper application of these techniques, we believe that it is possible to improve these results to a level where in the future we will be able to monitor the entire planet in (near) real-time, not only for earthquakes but also for volcanoes, landslides, ice poles control, among others.

4. Conclusion

In this paper, the application of deep learning to detect and segment the deformation fringes created by earthquakes in InSAR interferograms without any atmospheric correction was proposed.

We successfully created two InSAR datasets and applied them to train three state-of-the-art models, achieving a satisfactory result for the classification with an AUC of 0.864 for the VGG19 model.

We have exciting results for the segmentation models that open good perspectives for the future; however, more data is needed to improve the results until the level is desirable. In practice, the segmentation model Unet can find the location of earthquake fringes but is not good to isolate them from the rest of the image achieving a maximum of 0.5896 Dice Score.

Dual attention is not a good option to segment earthquake fringes in SAR interferograms and can be discarded in future works.

We believe that these results can be improved with a deeper application of artificial intelligence and more expansive data in the future. Until we have more positive data (with earthquake fringes), it can be deleted patches without deformation fringes, and this way, we reduce the unbalancing and maybe achieve better results.

Acknowledgements

This work is financed by National Funds through the Portuguese funding agency, FCT - Fundação para a Ciência e a Tecnologia, within project UIDB/50014/2020.

References

[1] M. E. Pritchard, "InSAR, a tool for measuring Earth's surface deformation," *Phys. Today*, vol. 59, no. 7, pp. 68–69, 2006, doi: 10.1063/1.2337843.

[2] Z. Lu, O. Kwoun, and R. Rykhus, "Interferometric synthetic aperture radar (InSAR): Its past, present and future," *Photogramm. Eng. Remote Sensing*, vol. 73, no. 3, pp. 217–221, 2007.

[3] E. A. Hetland, P. Musé, M. Simons, Y. N. Lin, P. S. Agram, and C. J. Dicaprio, "Multiscale InSAR Time Series (MInTS) analysis of surface deformation," *J. Geophys. Res. Solid Earth*, vol. 117, no. 2, pp. 1–17, 2012, doi: 10.1029/2011JB008731.

[4] Y. Lecun, Y. Bengio, and G. Hinton, "Deep learning," *Nature*, vol. 521, no. 7553, pp. 436–444, 2015, doi: 10.1038/nature14539.

[5] François Chollet, *Deep Learning with Python*, vol. 10, no. 2. 2018.

[6] M. V. Valueva, N. N. Nagornov, P. A. Lyakhov, G. V. Valuev, and N. I. Chervyakov, "Application of the residue number system to reduce hardware costs of the convolutional neural network implementation," *Math. Comput. Simul.*, vol. 177, pp. 232–243, 2020, doi: 10.1016/j.matcom.2020.04.031.

[7] C. M. J. Brengman and W. D. Barnhart, "Identification of Surface Deformation in InSAR Using Machine Learning," *Geochemistry, Geophys. Geosystems*, vol. 22, no. 3, p. e2020GC009204, 2021, doi: https://doi.org/10.1029/2020GC009204.

[8] N. Anantrasirichai, J. Biggs, F. Albino, P. Hill, and D. Bull, "Application of Machine Learning to Classification of Volcanic Deformation in Routinely Generated InSAR Data," *J. Geophys. Res. Solid Earth*, vol. 123, no. 8, pp. 6592–6606, 2018, doi: 10.1029/2018JB015911.

[9] N. Anantrasirichai, J. Biggs, F. Albino, and D. Bull, "A deep learning approach to detecting volcano deformation from satellite imagery using synthetic datasets," *Remote Sens. Environ.*, vol. 230, no. May, p. 111179, 2019, doi: 10.1016/j.rse.2019.04.032.

[10] S. Valade *et al.*, "Towards global volcano monitoring using multisensor sentinel missions and artificial intelligence: The MOUNTS monitoring system," *Remote Sens.*, vol. 11, no. 13, pp. 1–31, 2019, doi: 10.3390/rs11131528.

[11] J. Sun *et al.*, "Automatic Detection of Volcanic Surface Deformation Using Deep Learning," *J. Geophys. Res. Solid Earth*, vol. 125, no. 9, pp. 1–17, 2020, doi: 10.1029/2020JB019840.

[12] N. Anantrasirichai, J. Biggs, F. Albino, and D. Bull, "The Application of Convolutional Neural Networks to Detect Slow, Sustained Deformation in InSAR Time Series," *Geophys. Res. Lett.*, vol. 46, no. 21, 2019, doi: 10.1029/2019GL084993.

[13] Y. Wang *et al.*, "Ground deformation analysis using InSAR and backpropagation prediction with influencing factors in Erhai Region, China," *Sustain.*, vol. 11, no. 10, 2019, doi: 10.3390/su11102853.

[14] N. Anantrasirichai *et al.*, "Deep learning framework for detecting ground deformation in the built environment using satellite insar data," *arXiv*, pp. 1–22, 2020.

[15] P. Ma, F. Zhang, and H. Lin, "Prediction of InSAR time-series deformation using deep convolutional neural networks," *Remote Sens. Lett.*, vol. 11, no. 2, pp. 137–145, 2019, doi: 10.1080/2150704X.2019.1692390.

[16] B. Rouet-Leduc, R. Jolivet, M. Dalaison, P. A. Johnson, and C. Hulbert, "Autonomous Extraction of Millimeter-scale Deformation in InSAR Time Series Using Deep Learning," 2020, [Online]. Available: http://arxiv.org/abs/2012.13849.

[17] W. Weng and X. Zhu, "UNet: Convolutional Networks for Biomedical Image Segmentation," *IEEE Access*, vol. 9, pp. 16591–16603, 2015, doi: 10.1109/ACCESS.2021.3053408.

[18] "Adobe." https://www.adobe.com/pt/creativecloud.html?gclid=Cj0KCQjw3f6HBhDHARIsAD_i3D9GE9tPAnNxX-C61XuR4RxSvG2kJJxNFy6lFNsVFTAMEXyw1GHogIcaAlcPEALw_wcB&mv=search&mv=search&sdid=MQH8S7GK&ef_id=Cj0KCQjw3f6HBhDHARIsAD_i3D9GE9tPAnNxX-C61XuR4RxSvG2kJJxNFy6lFNsVFTAMEXyw1GHogIcaAlcPEALw_wcB:G:s&s_kwcid=AL!3085!3!276763743536!e!!g!!adobe!1447265403!61926049328 (accessed Jul. 27, 2021).

[19] T. Y. Lin, P. Goyal, R. Girshick, K. He, and P. Dollár, "Focal loss for dense object detection," *arXiv*, pp. 2980–2988, 2017.

[20] C. Szegedy, V. Vanhoucke, S. Ioffe, J. Shlens, and Z. Wojna, "Rethinking the Inception Architecture for Computer Vision," *Proc. IEEE Comput. Soc. Conf. Comput. Vis. Pattern Recognit.*, vol. 2016-Decem, pp. 2818–2826, 2016, doi: 10.1109/CVPR.2016.308.

[21] K. Simonyan and A. Zisserman, "Very deep convolutional networks for large-scale image recognition," *3rd Int. Conf. Learn. Represent. ICLR 2015 - Conf. Track Proc.*, pp. 1–14, 2015.

[22] K. He, X. Zhang, S. Ren, and J. Sun, "Deep residual learning for image recognition," *Proc. IEEE Comput. Soc. Conf. Comput. Vis. Pattern Recognit.*, vol. 2016-Decem, pp. 770–778, 2016, doi: 10.1109/CVPR.2016.90.

[23] Z. H. Hoo, J. Candlish, and M. D. Teare, "What is a ROC curve?," *Emerg. Med. J.*, 2017.

[24] Z. C. Lipton, C. Elkan, and B. Narayanaswamy, "Thresholding Classifiers to Maximize F1 Score," 2014, [Online]. Available: http://arxiv.org/abs/1402.1892.

[25] H. Guo, H. Liu, C. Wu, W. Zhi, Y. Xiao, and W. She, "Logistic discrimination based on G-mean and F-measure for imbalanced problem," *J.*

Intell. Fuzzy Syst., vol. 31, no. 3, pp. 1155–1166, 2016, doi: 10.3233/IFS-162150.